

Magnetar 1E1547.0-5408
in search for a pulsar wind nebula

Kimberly Jongman
Supervised by: dr. Jacco Vink

August 17, 2012



Image credit – John Rowe Animations. An artist's impressions of magnetar XTE J1810-197 (similar to 1E1547.0-5408) showing the radio pulses and the magnetic field.

Abstract

Around magnetar 1E1547.0-5408 extended emission was discovered. The question is: "Is this a pulsar wind nebula or is it dust scattering?". Here I try to give an answer. I looked at properties of the star, investigated the spectrum of the source and the extended emission and looked at the radial profile. From the spectrum I calculated the hardness ratio and fractional intensity. And the radial profile was fitted with a dust scattering model.

From the radial profile we might conclude there is more than dust scattering. But this is not very conclusive. The fractional intensity shows there is more than dust scattering for the inner region of the extended emission, but not beyond 40". Previous research showed emission other than dust out to at least 150". And the source was a lot brighter at the time of the observation than in 2006, data to which this research is compared. This gives many problems and might explain some observational differences.

Contents

1	Introduction	3
2	Discovery	4
3	Magnetars	6
3.1	What are magnetars?	6
3.2	Bursts	8
3.3	Glitches	8
3.4	Characteristics of pulsars	9
3.5	Dead magnetars	11
3.6	Magnetar models	11
4	1E1547.0-5408	12
4.1	Source	12
4.2	Extended emission	13
4.2.1	Pulsar wind nebula	13
4.2.2	Dust scattering	13
4.3	Outbursts	14
4.4	Rings	14
4.5	Supernova remnant	14
4.6	Radio emission	14
5	Data analysis	15
5.1	Satellites	15
5.1.1	Chandra	15
5.1.2	XMM Newton	15
5.1.3	SWIFT	15
5.2	Data sets	16
5.3	Lightcurve	17
5.4	Spectra	18
5.4.1	Pile up	19
5.4.2	Extended emission	22
5.5	Flux	23
5.6	Hardness ratios	25
5.7	Fractional intensity	26

5.8	Radial profile	27
5.8.1	Draine model	27
5.9	Radial profile	29
5.9.1	2011 data	29
5.10	Rings	30
6	Discussion	33
7	Conclusions	34

Chapter 1

Introduction

During the second year bachelor course Electrodynamics we had to write a report on an application of the things we learned. The course was very theoretical and this report would show us the practical side of it. Since I am very interested in astronomy, I looked for electrodynamics and magnetism in stars. This is how I learned about magnetars, stars with extreme magnetic fields. I found out there wasn't much known yet and these stars were still a big mystery. This kept intriguing me. Luckily dr. Jacco Vink had written some papers on this subject. One of the most recent papers was on the extended emission around one of the known magnetars and there was new data available at the time I started working on my thesis. This all led to the perfect subject for a year of research.

Around magnetar 1E1547.0-5408 a pulsar wind nebula was detected by Vink & Bamba (2009), but the X-ray observation used was short. They requested a longer observation to get a better look at the data. At the same time, also radio data were requested from ATCA, since a pulsar wind nebula would also be visible in this band. During this research project I analyzed the X-ray data. First I will give an introduction on magnetars in general, what we know so far and how they were discovered. Then I will describe this specific source, what are its characteristics and what do we already know from many other observations. Last I will describe the analysis of the data and the comparison with archived data. To see if we are dealing with a pulsar wind nebula or dust scattering, I will look at a dust scattering model. Since there are many points of discussion, I will also discuss some of these points.

Chapter 2

Discovery

In the 1960s, during the Cold War, the US defense department launched the Vela satellites to search for gamma rays. They feared that the Soviet Union was doing nuclear tests in outer space. To test this, the US sent out satellites to look for gamma-rays sent out by the explosions. No nuclear tests were observed, but they did detect many brief gamma-ray bursts scattered across the sky. The bursts had to come from stars.

In January 1979 the first big burst of gamma rays was detected from a Soft Gamma Repeater (SGR) in the constellation Sagittarius. Only two months later an even bigger burst was detected. On March 5, 1979, two Soviet space probes, Venera 11 and Venera 12, were hit by an enormous flux of gamma rays. The onboard gamma ray detectors usually read 100 counts per second background noise, now the radiation level went off scale, above 200,000 counts. 11 seconds later another space probe, Helios 2, was hit by a gamma ray burst. A plane wave front of high energy radiation traveled through the solar system, hitting every detector on its way with a pulse of 0.2 seconds of gamma ray radiation. The pulse was 100 times higher than any previous burst ever detected from outside our galaxy. Since nobody had any idea what could cause such a high pulse, it was classified as a gamma ray burst (GRB). After the high pulse, a fainter tail of soft gamma rays followed, lasting 3 minutes. There appeared to be cycles of pulses for those 3 minutes, repeating every 8 seconds. Over the next 4 years another 16 bursts were detected, but none of these as intense as the first. In May 1983, the last burst was detected from this source.

First it was assumed that the source was in the Milky Way, fairly close to Earth, because the source was so bright. This meant that the luminosity was just below the Eddington limit. But since many satellites detected the burst, its position in the sky could be determined. This put the source at a distance 1000 times further away, in the Large Magellanic Cloud. Therefore it was actually 1 million times brighter, exceeding the Eddington limit by far (Kouveliotou, Duncan and Thompson, 2003).

The burster had strange properties. For instance, it was an isolated neutron star within a supernova remnant, the source was less than 10,000 years young and emitting X-rays from an unknown energy source. Many theories were proposed, but they all explained some of the properties, not all. After these observations more telescopes, observing at different wavelength bands, were launched to search for more of these interesting objects.

Not only were SGRs finally classified as magnetars, but also Anomalous X-ray Pulsars (AXPs). These sources were discovered as point sources in supernova remnants. They were not bursting, so a new category of anomalous X-ray pulsars was created. The distinction between AXPs and SGRs became less sharp when also AXPs started showing bursts. And better data showed their peculiar properties to be even more similar to the SGRs. Therefore the magnetar model is now applied to both types of neutron stars.

Chapter 3

Magnetars

3.1 What are magnetars?

Stars with a mass between 8 and 20 M_{\odot} die in a supernova explosion. In this case the stellar core implodes into a very dense star consisting of neutrons, because during the collapse protons and electrons in the core combine into neutrons. The stellar envelope is blown away, leaving a neutron star with a radius of approximately 12 km. There is no further collapse of the core possible and the star is stable. Pulsars are fast rotating neutron stars with a high magnetic field and send out energy through beams. If Earth happens to be in the path of a beam of radiation emitted from the neutron star, we can observe the pulsars. Otherwise we would not be able to see them (lighthouse effect).

Pulsars have a high magnetic field compared to magnetic fields we can achieve on Earth. To demonstrate this, here is a table of the scales of magnetic fields known in the universe. As can be seen, the magnetic field of Earth is low, the field strength of a pulsar is very high, but the field strength of a magnetar is extremely high, even higher than the quantum electrodynamic field strength.

Earths magnetic field	0.6 G
Common magnet	100 G
Lab-made magnet	5×10^5 G
Radio pulsar	$10^{12} - 10^{13}$ G
B_Q	4.4×10^{13} G
Magnetars	$10^{14} - 10^{15}$ G

Table 3.1: List of magnetic field strengths from very low to the magnetar strength.

The quantum electrodynamic field strength, called B_Q , equals $\frac{m_e^2 c^3}{e \hbar}$. The extreme magnetic fields in magnetars, higher than B_Q , have an impact on the matter and radiation in the fields. The electrons in atoms do not follow a circular orbit any more, but the orbits become elongated. At field strengths above 10^{14} gauss, which happens in magnetars, a hydrogen atom becomes 200 times narrower.

The speed of polarized light in extreme magnetic fields changes and thus the wavelength changes. At magnetic fields higher than B_Q , X-rays can merge together or split into two.

Also scattering can be suppressed when the electrons cannot vibrate. A light wave can pass the electrons freely when the electrons are stuck in the field.

Because the magnetic field in a magnetar is so extremely high and the magnetic field strength in a common pulsar is below B_Q , we can compare the two types of stars and see the influence of the extremely high magnetic fields (All above information came from Kouveliotou, Duncan and Thompson 2003).

Anomalous X-ray Pulsars are one type of magnetars and since 1E1547.0-5408 is classified as an AXP, this will be the main type discussed from now on. AXPs are different from accretion-powered pulsars. X-rays from the pulsars come from the accretion of matter from one star onto the other. Magnetars do not have a binary companion. Therefore accretion is not the source of X-rays.

Normal pulsars are created when the initial neutron stars spin slowly and have a high magnetic field, on the order of 10^{12-13} gauss. But when the star rotates faster, it can become a magnetar, with high magnetic field and twisted field lines. More on this will follow in the section on magnetar models (section 3.6).

Also magnetars differ from normal pulsars by their spin periods. Pulsars have spin periods ranging from milliseconds to hours; the period range for magnetars is much smaller, from 2 to 12 seconds. This could be due to observational limitations, but it can also, in part, be explained theoretically. Faster rotating magnetars, smaller period, could be excluded due to a rapid spin-down on a timescale of 10^3-10^4 year. A limit on slower rotating magnetars might be connected to the decay of the magnetic field.

The spectra of magnetars are best fitted with a blackbody spectrum and a steep power law. There is no theory on why this is the best fit, this is just a phenomenological description. The best fits do indicate that the soft X-ray spectrum (below 10 keV) is more complex than a simple Planckian function. This is probably the result of the strong magnetized atmosphere of magnetars. Counterparts for the Soft Gamma-ray repeaters share many properties with AXPs, similar luminosities, periods and period derivatives, but they have a harder spectrum.

The luminosities of magnetars are higher than those of many known weak radio pulsars, so it was expected that the magnetars would be visible in the radio. But early observations gave no results during the search for them in the radio bands. Therefore it was thought that it was a property of magnetars to have no radio emission. But later, in 2004, a radio source was found for XTE J1810-197. And in 2007 radio emission was seen from magnetar 1E1547.0-5408. So far, these are the only two magnetars observed in the radio. It is also remarkable that the radio-emitting magnetars are the two with the smallest periods (Camilo et al., 2007).

3.2 Bursts

Neutron stars are made up of mainly neutrons (90%), but they also contain protons and electrons, electrically charged particles. This configuration is stable due to the high pressure and temperature. At the surface of the star the pressure and temperature drop very quickly, but the gravitational force is still very strong. This causes a crust to form on the surface where heavy particles arrange in a quasi-cubic lattice with electrons flowing freely between them (Ruderman, 1969). In pulsars this crust is stable, but in magnetars the magnetic field stresses the charged crust and deforms the surface, allowing the magnetic field lines to move and twist. This formation can become unstable and burst, releasing a tremendous amount of energy. A burst will last for no longer than 1 second. But where exactly the stress is built-up, is not yet known. It is also possible it builds up in the interior of the star.

By now, many bursts have been detected on magnetars. This appears to be part of the life of magnetars (Mereghetti, 2008).

3.3 Glitches

The bursts described before are caused by stress in the magnetar, the stress is released through a big burst. This moves the star's surface, but also the core. The release of stress causes Alfvén waves in the magnetosphere. This whole process can make the star speed up (glitch) or slow down (anti-glitch) in rotation. Glitches have been observed in almost all AXPs. The properties of these glitches are the same as for young pulsars. From this we can conclude that magnetars are similar to young pulsars and are therefore young. Not all observed glitches were accompanied by bursts, but all bursts were accompanied by a glitch, or in some rare cases, an anti-glitch.

3.4 Characteristics of pulsars

If we assume a mass of $1.4 M_{\odot}$ and a radius of 10 km, which are normal values for pulsars, we can calculate some characteristics of magnetars (following Cordon & Ransom 2010).

Let us start with the energy and energy lost due to rotation.

The moment of inertia I for a sphere and magnetar is given by

$$I = \frac{2}{5}MR^2 \approx 1.12 \times 10^{45} \text{g cm}^2. \quad (3.1)$$

This we can use to calculate the rotational energy and the energy lost through this rotation is the change in rotational energy

$$\begin{aligned} E_{rot} &= \frac{1}{2}I\Omega^2 = \frac{2\pi^2 I}{P^2} \approx 5.5 \times 10^{45} \text{ergs}, \\ \dot{E}_{rot} &= I\Omega\dot{\Omega} = \frac{2\pi}{P} \frac{2\pi\dot{P}}{P^2}. \end{aligned} \quad (3.2)$$

We can also estimate the rotational power using the Larmor equation

$$P_{rad} = \frac{2q^2\dot{v}^2}{3c^3} = \frac{2}{3} \frac{(q\ddot{r} \sin \alpha)^2}{c^3} = \frac{2}{3} \frac{\ddot{p}_{\perp}^2}{c^3} \quad (3.3)$$

for radiation from a rotating electric dipole. Where P is power, q is electric charge, v is velocity of a nonrelativistic point charge, α is the angle between acceleration and observation and $\ddot{p} = q\dot{V}$. For the radiation of a magnetic dipole we can replace \ddot{p}_{\perp} with \ddot{m}_{\perp} with $m = BR^3 = m_0 e^{-i\Omega t}$ so that $\ddot{m} = \Omega^2 m$. We also use an inclination of the magnetic dipole α from the rotation axis.

This gives

$$P_{rad} = \frac{2}{3c^3} (BR^3 \sin \alpha)^2 \left(\frac{2\pi}{P}\right)^4. \quad (3.4)$$

Now we assume $P_{rad} = -\dot{E}$ and we can get an estimate of the magnetic field strength (B_{\perp})

$$\begin{aligned} P_{rad} &= -\dot{E} \\ \frac{2}{3c^3} (BR^3 \sin \alpha)^2 \left(\frac{2\pi}{P}\right)^4 &= \frac{2\pi}{P} \frac{2\pi\dot{P}}{P^2} \\ B^2 &= \frac{3c^3 I}{8\pi^2 R^6 \sin^2(\alpha)} P\dot{P} \\ B &> \left(\frac{3c^3 I}{8\pi^2 R^6}\right)^{1/2} (P\dot{P})^{1/2} \\ B &> 3.2 \times 10^{19} (P\dot{P})^{1/2}. \end{aligned} \quad (3.5)$$

We assume that

$$P\dot{P} = \frac{8\pi^2 R^6 (B \sin \alpha)^2}{3c^3 I} \quad (3.6)$$

doesn't change with time. When rewriting from $P\dot{P} = \dot{P}P$ to $PdP = P\dot{P}dt$ and integrating:

$$\int_{P_0}^P PdP = P\dot{P} \int_0^{\tau} dt \rightarrow \frac{P^2 - P_0^2}{2} = P\dot{P}\tau. \quad (3.7)$$

If P_0 is much smaller than P , then

$$\tau = \frac{P}{2\dot{P}}. \quad (3.8)$$

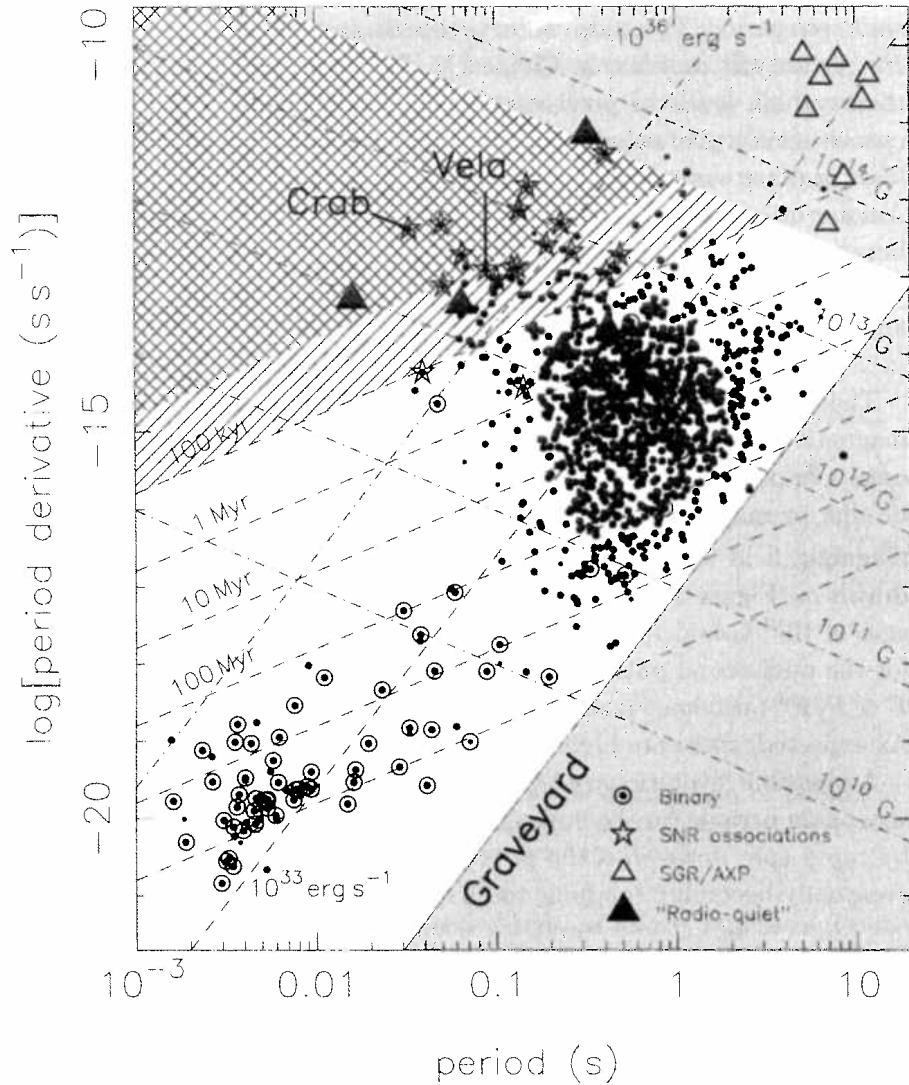


Figure 3.1: The $P-\dot{P}$ diagram. In the middle are the normal pulsars, the lower left corner the binary pulsars and in the upper right corner the magnetars (from Handbook of Pulsar Astronomy, Lorimer & Kramer (2005)).

The $P\dot{P}$ diagram in figure 3.1, gives a lot of information about pulsars. It gives information about the age, magnetic field strength and spin-down power, just by knowing P and \dot{P} . Based on the previous equations, you can follow the life of a pulsar in this diagram. After the supernova explosion the pulsar appears in the upper right corner of the diagram. If B is conserved, they gradually move down along the line of constant B . Once they cross the "death line" in the diagram, they no longer radiate radio pulses and they become difficult to observe. In the lower left corner we find the pulsars in binary systems. They are spun-up by mass accretion from the donor star and the angular momentum transfer. In the upper right corner are the SGRs and AXPs, including the magnetars. As we see, magnetar 1E1547.0-5408 fits in this region with $P=2.01$ s and $\dot{P} = 2.3 \times 10^{-11}$.

3.5 Dead magnetars

The process of dissipation of the magnetic energy of magnetars will not go on forever. Once the temperature drops below an (unknown) threshold, the dissipation shuts down very quickly. Then the magnetars are no longer visible, since they do not radiate X-rays anymore and their bursts are too small to detect. This suggests there are also many dead magnetars, but we are not yet able to detect them with the current telescopes. Where they are located, depends on their initial velocity through space. All observed magnetars (except for one) are located in the Galactic disk, but if they have a high velocity, they can also end up in the halo.

3.6 Magnetar models

The origin and evolution of magnetars is still unknown. One of the possible ways to create a magnetar is the so-called dynamo theory. In 1993, Thompson & Duncan calculated that if the birth spin period of pulsars is in the order of tens of milliseconds, a magnetic field of $3 \times 10^{17} \left(\frac{1\text{ms}}{P_0}\right)$ gauss is possible. For the amplification of the seed field, rapid neutrino cooling is necessary in driving the strong turbulent convection. This dynamo will only work for 10 seconds, but it is able to generate extremely strong magnetic fields. However it does require magnetars to be born with millisecond periods. This would be visible in a large spatial velocity, in the order of 10^3 km/s and the associated supernova remnant should be more energetic than normal core collapse supernovae. The supernova remnant should be a hypernova remnant. Observations so far have not indicated that magnetars have a high spatial velocity and also the high supernova energy is not fulfilled in many cases (Vink & Kuiper, 2006). This theory cannot yet fully be dismissed, but it leaves room to other theories.

One of these other models is the so-called fossil field model. This model is based on conservation of magnetic flux. If we have a high mass star with a high magnetic field, then after the supernova explosion, we are left with a smaller star, but the magnetic flux should be conserved. This theory is known for white dwarfs and might also be applied in magnetars.

Even though there are many possible birth models for magnetars, it is not yet known which one is the correct model.

Chapter 4

1E1547.0-5408

4.1 Source

The first observations of 1E1547.0-5408 were made with the Einstein X-ray satellite. It was discovered during a search for X-ray counterparts of unidentified gamma-ray sources (Lamb & Markert, 1981). The source can be found at coordinates 15 50 54.11 ; -54 18 23.7, or in galactic coordinates 327.2370 -00.1316. This shows that the magnetar is in the galactic plane.

The star was identified as a magnetar by Gelfand & Gaensler (2007) in the supernova remnant G327.24-0.13. In 2007, Camilo et al. detected the pulsation period $P = 2.069$ sec. and a period derivative $\dot{P} = (2.318 \pm 0.005) \times 10^{-11}$ with the use of the Parkes radio telescope. With the equations from section 3.4 we can calculate the expected magnetic field strength of the magnetar and its age. We get a lower limit on the magnetic field strength of 2.2×10^{14} gauss and an age of 1385 years.

There is still some debate about the distance to the source. Using the free-electron model of Cordes & Lazio (2002) the distance is 9 kpc (Camilo et al., 2007). But the source is also related to supernova remnant SNR G327.24-0.13, which is positioned at a distance of 4 kpc (Gelfand & Gaensler, 2007). Also the rings, occurring after the 2009 outburst, place the source at a distance of approximately 4 kpc.

We can also see that the measured luminosity $L_x \sim 10^{-12}$ ergs/s/cm² is more than estimated from $I\Omega\dot{\Omega}$ ($= 3.1 \times 10^{35}$ ergs s⁻¹). If we assume an X-ray efficiency of 10^{-4} (Kargaltsev & Pavlov 2008) and a distance of 4 kpc (the lower limit of the distance to magnetar 1E1547.0-5408), we should observe a flux of 1.62×10^{-13} ergs/s/cm². So we need something extra to create the extra energy loss.

4.2 Extended emission

In 2009 Vink & Bamba wrote on the existence of a pulsar wind nebula around magnetar 1E 1547.0-5408. The extended emission consisted of an inner part of 45" and an outer part out to 2'.9, which coincides with the supernova remnant previously detected. It was discovered by accident as they were trying to find a X-ray counterpart for the radio shell of the supernova remnant. In archival data of Chandra from 2006, a faint but distinct extended source was observed. The data were compared to a semi-analytical dust scattering model from Draine (2003), from which can be concluded that the dust is not the dominant part of the emission. In 2009 they stated deeper observations were needed. In this research project I used these deeper observations to further constrain properties of the extended emission.

4.2.1 Pulsar wind nebula

A pulsar wind nebula (PWN) is a bubble of shocked relativistic particles, produced when a pulsar's wind interacts with its environment (Gaensler & Slane, 2006).

A good example of a pulsar wind nebula is the Crab nebula. This nebula is centrally filled at all wavelengths, whereas normal supernova remnants are shell like. This nebula is thus different from other supernova remnants. The nebula's energy is dominated by particles flowing away from the central source, ejected long after the supernova explosion. After the discovery of this extended source, a theory was developed in which the source generates a magnetized particle wind energized by the spin-down power. The central source in the Crab nebula is a pulsar, hence a pulsar wind nebula. The size of the PWN decreases as you look at higher energies, because the energy is radiated away before it can travel to the outer edges of the nebula.

In some cases the PWN is surrounded by a shell-like supernova remnant, but this is not always visible. For instance, around the Crab nebula no shell is seen. Many PWNe have a well-defined source and are spatially resolvable, we can study them in great detail and they help us understand a wide range of astrophysical problems.

In general, the \dot{E} of a pulsar is between 3×10^{28} and 5×10^{38} ergs s^{-1} . In the case of $\dot{E} > 4 \times 10^{36}$ ergs s^{-1} a pulsar wind nebula can be created (Gotthelf, 2004). And pulsars with a magnetic field strength between 1×10^{12} and 5×10^{13} gauss show the most prominent PWNe.

The X-ray emission (which we will investigate in this research project) can best be described with a power law index of $\Gamma \approx 2$ (Gaensler & Slane, 2006). We can divide the X-ray intensity, from the spectral fitting, by the rotational energy loss, $\eta_X \equiv L_X/\dot{E}$. This gives an efficiency factor of how much rotation energy goes into X-rays; $\eta_X \approx 10^{-4} - 10^{-3}$, in general.

4.2.2 Dust scattering

Within galaxies there is a lot of dust, also in our own galaxy. For example, we have a hard time investigating the center of our galaxy because of the tremendous amount of dust. The source we are looking at for this research is in the galactic plane and thus lightly obscured by dust. The interstellar dust grains larger than $0.1 \mu\text{m}$, absorb and scatter X-rays and with this creating a halo around the source. This affects the observation we do in the X-ray band, but nearly every band is affected by the dust particles. The nature of these stellar dust grains remains uncertain, but there are some candidate materials. Silicates and carbonaceous materials contribute greatly, but also SiC, CaCO_3 and $\text{CaMg}(\text{CO}_3)_2$ are found in the interstellar dust.

4.3 Outbursts

On October 3, 2008, Swift detected several outbursts of magnetar 1E1547.0-5408. After this series of outbursts the X-ray flux was increased to a maximum of $6.3 \pm 0.5 \times 10^{-11}$ ergs cm² s⁻¹. This was not the biggest outburst of this source. A few months later, in 2009, there was another major outburst. On January 22, 2009 the source underwent even stronger outbursts than in 2008, again detected by Swift and also Fermi. And this time the flux also increased. Within a few hours after the first detection, over 200 smaller bursts were detected.

In total 3 outburst periods were recorded, each consisting of many outbursts, making this one of the most active magnetars.

During or just prior to the observation of 2011 there was no outburst detected by any satellite.

4.4 Rings

After the January 2009 bursts, Swift/XRT and XMM-Newton/EPIC observations showed three concentric rings around 1E 1547.0-5408. When dust is concentrated in a thin layer and the star bursts in X-rays, the halo of dust can appear as a ring. Rings of dust have been observed at other GRBs before. The rings around 1E1547.0-5408 were not visible anymore after a week, so a long 50 ks observation was requested with XMM-Newton. Careful analysis by Tiengo et al. 2010 showed that the rings were clearly visible in this new observations, and also in the radial profile made from this observations. The rings showed up as peaks on top of the normal profile.

4.5 Supernova remnant

In 2007, Gelfand & Gaensler presented a paper on the (then still) candidate magnetar and an associated supernova remnant. The compact source was 1E1547.0-5408 and the supernova remnant was the radio shell G327.24-0.13. They looked at multiple datasets from multiple wavebands (X-ray, radio, near-IR). The observed candidate magnetar is at the center of the SNR. This led to the conclusion that the star is a neutron star, which is extra evidence for the source being a magnetar and it was no longer just a candidate.

This observation, where the SNR and magnetar were associated, led to more constraints on the origin of magnetars; they are the result of a supernova explosion.

4.6 Radio emission

In 2006, XTE J1810-197, a different AXP, was detected in radio, but no other magnetar was visible in the radio band. In 2007 Camilo et al. detected magnetar 1E1547.0-5408 with the Parkes telescope in Australia, a radio telescope. This makes this source the second magnetar detected that emits radio waves. The observations were done on June 8, 2007, but the area containing the source was previously observed in 1998. At that time the source was not detected, suggesting that the source was at least 5 times fainter in 1998 than in 2007. When the data were compared with the radio data of the other radio emitting magnetar, Camilo et al concluded that the radio emission is triggered by X-ray outbursts of usually quiescent magnetars.

Chapter 5

Data analysis

5.1 Satellites

5.1.1 Chandra

Chandra X-ray observatory was launched in July 1999. It has four science instruments, ACIS: Advanced CCD Imaging Spectrometer, HRC: High Resolution Camera and the HETGS and LETGS: High and Low Energy Transmission Grating Spectrometer. The ACIS is the instrument I will be using for the data analysis. It can make X-ray images and at the same time it measures the energy of each incoming X-ray. It has an angular resolution of 0.5 arcseconds.

5.1.2 XMM Newton

In December 1999, XMM Newton was launched to observe the sky in X-rays. XMM stands for X-ray Multiple Mirrors, the telescope consists of three X-ray telescopes, two of the detectors are metal oxide semi-conductor (MOS) CCD arrays and the third is a pn camera. The MOS detectors work very well in the weak X-ray range. It is designed to detect X-ray emission from objects in the Solar System, star formation, formation and evolution of galaxy clusters, supermassive black holes and mapping of dark matter.

5.1.3 SWIFT

SWIFT is a gamma ray burst detector launched in 2004. It has three instruments, BAT, XRT and UVOT, which together observe in the gamma ray, X-ray, UV and optical wavebands and scan the sky continuously. In 2009 magnetar 1E1547.0-5408 showed a series of outbursts, detected by SWIFT. First the Burst Alert Telescope (BAT) detects the burst, then the position is determined and the telescope is pointed to the bursting source to observe the afterglow. This all happens within approximately 90 seconds. Among the mission goals are determining the origin of GRBs, to use them to expand the understanding of the young universe and do all-sky surveys.

5.2 Data sets

For this project I used many data sets. From Chandra I used the data set from 2011-06-02. This was the new observation requested by Vink and Bamba. It lasted 96515 seconds with the ACIS instrument, in timed mode, under observation id 12554.

I also used a observation of 2006-07-01, with principal investigator Gaensler. This was an exposure of 95322 seconds, also with the ACIS instrument in timed mode, under observation id 7287.

The data from Chandra were processed using CIAO 4.3 (Fruscione et al., 2006).

From XMM-Newton I used 5 data sets from 2004 to 2010. 2004-02-08 with PI Slane, 2006-08-21 with PI Gaensler, 2007-08-09 with PI Schartel, 2009-02-03 with PI Schartel and finally 2010-02-10 with PI Kaspi.

And from SWIFT I did not use data directly, but I checked to see if there was a detection of a burst during the observation with Chandra in 2011.

Beside these data sets I used for this analysis, I also used conclusions other scientists made from even more data sets.

When having a closer look at the image (figure 5.1), we notice a few things. First of all we see that the source is really bright, but there is also clearly extended emission. The yellow inner part is the source, but the surrounding pink and green is the extended emission. This is also very bright. We also see a line from north-west to south-east across the image (figure 5.2). This line is due to the photons that hit the detector during read-out. This line is included in the analysis of the data, but it is also part of the background. Therefore this should not be a problem.

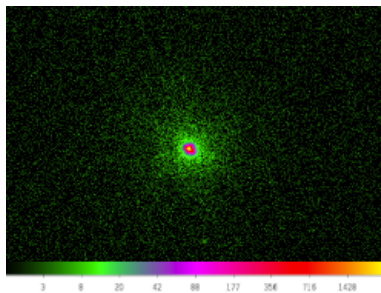


Figure 5.1: The Chandra observation of the source in 2011. Colors show amount of photons. Yellow is the source, pink and green the extended source.

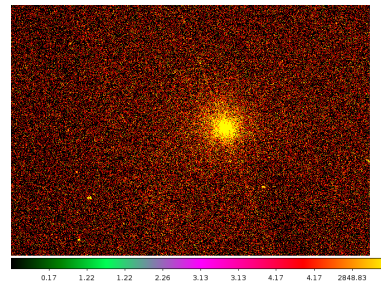


Figure 5.2: The Chandra observation, in a different color scheme, to show the line from the read-out. In this color scheme the source and the extended emission can not be seen separately.

5.3 Lightcurve

First I looked at the lightcurve of the Chandra data of 2011. This can give information about the behavior of the magnetar during the observation. It tells us about the variability of the source or if there is a flare during the observation. This is done with a simple tool in CIAO, called dmextract. This creates a table with counts per second in the defined region. After extracting the data, I used IDL to plot the data.

Here I made lightcurves of the inner 0.5" and 1" and also from 1-40". The first two lightcurves give information about the source and the 1-40" area tells us something about the variability of the extended emission. I have taken the full energy range of Chandra and used a bin time of 10 seconds. This is more than the 3.24 seconds between read-outs.

Figure 5.3 shows the lightcurves. There seems to be no variability in the source, not within the errors and especially no flares or bursts during the observation. So we don't have to take this into account while analyzing the data.

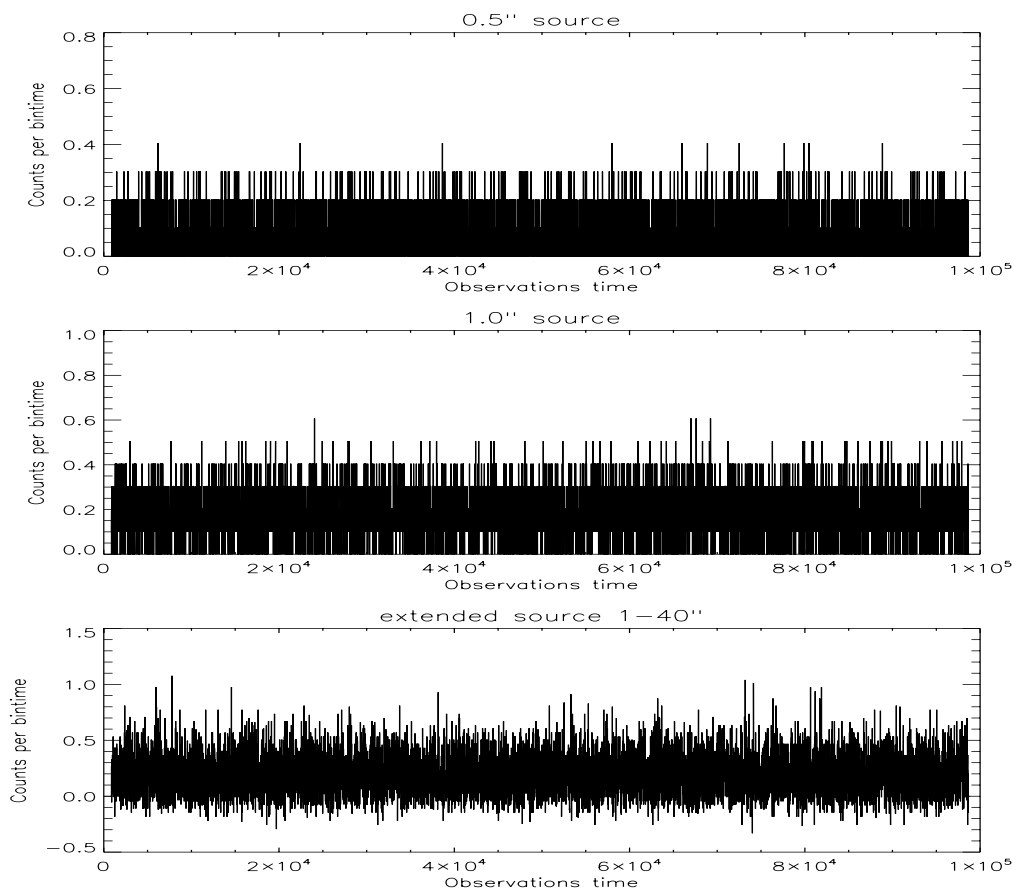


Figure 5.3: Lightcurve of the data with bin time 10 seconds, for inner 0.5" and 1.0" and for the extended source from 1"-40". The figure is cluttered, but it does show there are no outbursts during the observation.

5.4 Spectra

The XMM Newton data were processed using SAS 11.0.0 science threads for ‘Extraction of MOS/PN spectra from point-like sources’.

The data from Chandra were processed using CIAO 4.3 science thread for ‘Extracting Spectrum and Response Files for a Point-like Source’ and ‘for extended sources’. By using a combination of CIAO tools, we can extract the spectra for the background and source for point sources as well as the extended sources. Also the appropriate Response Matrix Files (RMF) and Ancillary Response Files (ARF) are created. These are needed for the correct spectrum weighted by telescope area and detector efficiencies for different energies. This can all be automated with a script with input of the file, region and background area. A Response Matrix File corrects for the spreading of the observed counts by the detector resolution, since detectors are not perfect objects. And an Ancillary Response File combines the quantum efficiency and the effective area as a function of energy averaged over time. If the detector was perfect, the distribution of counts that would be seen, is just the spectrum times the ARF.

Next I used XSpec 12.7.0 for the plots and fitting of the models.

The models used for the archived data are tbabs (an absorption model) with a power law and a blackbody component. These components give the best fits to magnetars, but it is unclear why exactly. For the 2011 data I had to add the pile-up model.

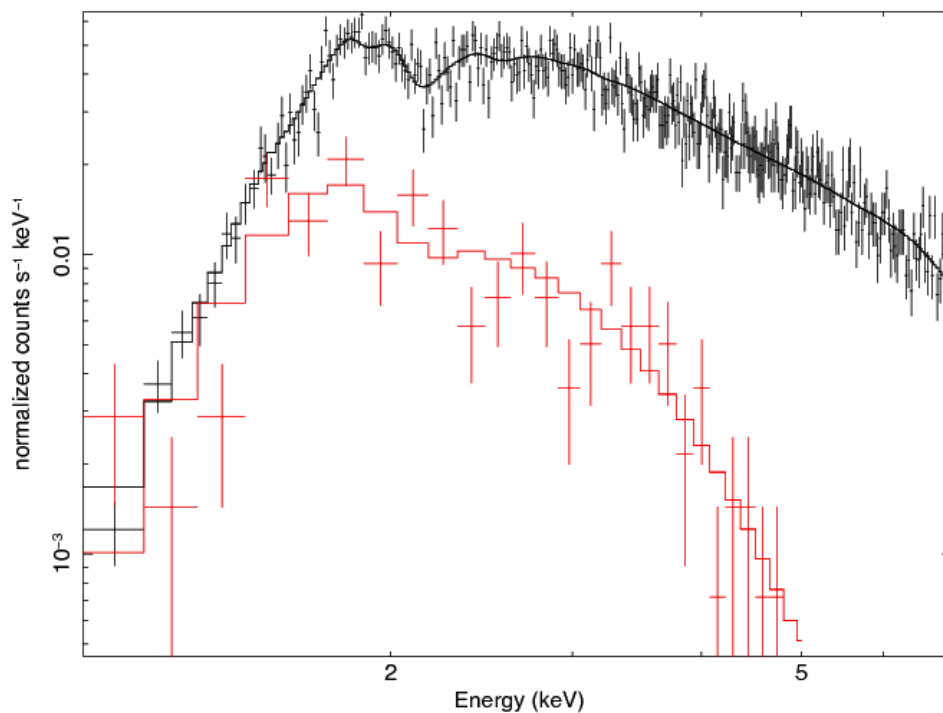


Figure 5.4: In black the spectrum for 2011 and in red the 2006 data. Here we see an excess of emission at higher energies for 2011, compared to 2006. This led to the idea of pile up.

5.4.1 Pile up

From the 2011 Chandra spectrum in figure 5.4 we see something odd. At the higher end of the spectrum there appear to be much more photons than expected from older spectra. The shape is very different, the spectrum is much steeper there. This could mean a few things; for one, something has happened to the magnetar and it now emits much more high energy photons; or two, the source was too bright and we have pile up. This happens when between read-outs of the CCD multiple photons hit the same spot on the detector, but this is seen as one event. Take multiple photons of low energy and take this to be one event, then this event has an higher energy than expected. If this is the case, can be checked (Davis, 2001).

CIAO has the possibility to make a pile up map. This map gives an indication of the amount of pile up and the places on the detector that have pile up. The map from the 2011 data (figure 5.5 right) showed that there was possibly a very small amount of pile up at the center of the source, but even more in the halo surrounding the source. The outer circle has a radius of $2.5''$. Since I only looked at the source, this would tell me there is no pile up there, which is odd. But this is exactly what happens in the case of severe pile up, since "in a severely piled-up case, the counts image can form a 'crater' where the apparent pile up is low. There should be a halo around this crater with a larger pile up indicator." From this I concluded that this is the case here and we have a severely piled up case. There is also a spot outside the source that shows pile up marked by the smaller circle. In the observation not many photons are observed, so pile up is not the case there. In the pile up model a parameter called α appears. Alpha parameterizes "grade migration" in the detector, and represents the probability, per photon count greater than one, that the piled event is not rejected by the spacecraft software as a "bad event". Specifically, if n photons are piled together in a single frame, the probability of them being retained (as a single photon event with their summed energy) is given by $\alpha^{(n-1)}$.

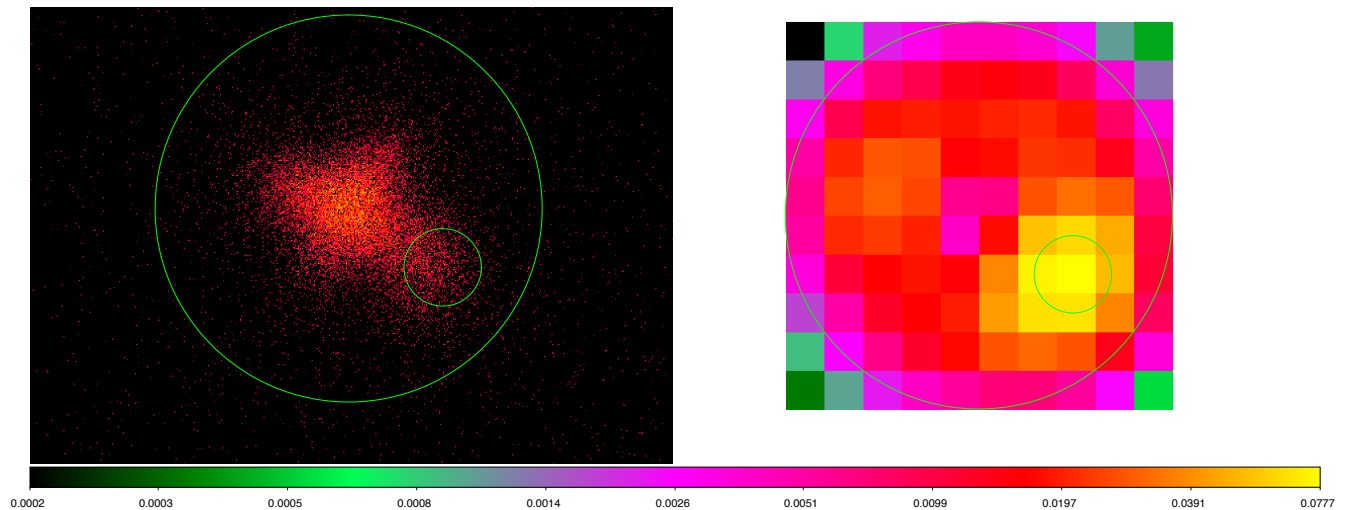


Figure 5.5: Left: Image of the source with the larger circle the extraction region for the pile up map. Right: The pile up map from CIAO. In the center the pile up fraction is 1-5% and in the smaller circle the pile up fraction is $>10\%$. The outer circle has a radius of $2.5''$.

For the comparison of the spectra from 2006 and 2011 I used the XSpec model tbabs (an absorption model) with a power law and a blackbody model. The parameters are hydrogen column density n_H , a power law and temperature in keV. I assume there is no change in n_H between 2006 and 2011. This gives a best fit value of $(3.37 \pm 0.12) \times 10^{22} \text{ cm}^{-2}$, giving a negative power law parameter for 2011, -1.7. Because of this value, we assumed something was going on. This all led to the idea of pile up.

The best fit value for n_H after the pile-up check is $(3.25 \pm 0.06) \times 10^{22} \text{ cm}^{-2}$. This gives an improvement on the power law parameter, now it is 1.53 ± 0.48 .

Data 2006

n_H	10^{22} cm^{-2}	3.37	\pm	0.12
PhoIndex		3.78	\pm	0.63
kT	keV	0.41	\pm	0.07
C-Statistic	= 0.82			

Table 5.1: Best fit for 2006 Chandra data of 1E1547.0-5408 for XSpec absorption model tbabs with a power law and blackbody.

Data without pile-up model 2011

n_H	10^{22} cm^{-2}	3.37	\pm	0.12
PhoIndex		-1.71	\pm	0.27
kT	keV	0.59	\pm	0.02
C-Statistic	= 1.04			

Table 5.2: Best fit for 2011 data without a pile up model, but with tbabs, power law and blackbody.

Data with pile-up model 2011

α		0.48	\pm	0.07
n_H	10^{22} cm^{-2}	3.25	\pm	0.06
PhoIndex		1.53	\pm	0.48
kT	keV	0.56	\pm	0.03
C-Statistic	= 1.04			

Table 5.3: Best fit for 2011 with the XSpec pile up model, tbabs with power law and blackbody.

The following sections are to compare the new data with the data analyzed in the paper by Olausen et al. (2011). This paper dismisses the pulsar wind nebula theory by analyzing the hardness ratio and fractional intensity. There they use different regions. Their data mainly consist of XMM data. The source they used is from 0 - 10". Then region A is from 20 - 40" and region B is from 40 - 150". I also included a region 0, from 10 - 20". In this last region, the effect of dust scattering should be highest. For a better view of the regions, see figure 5.6.

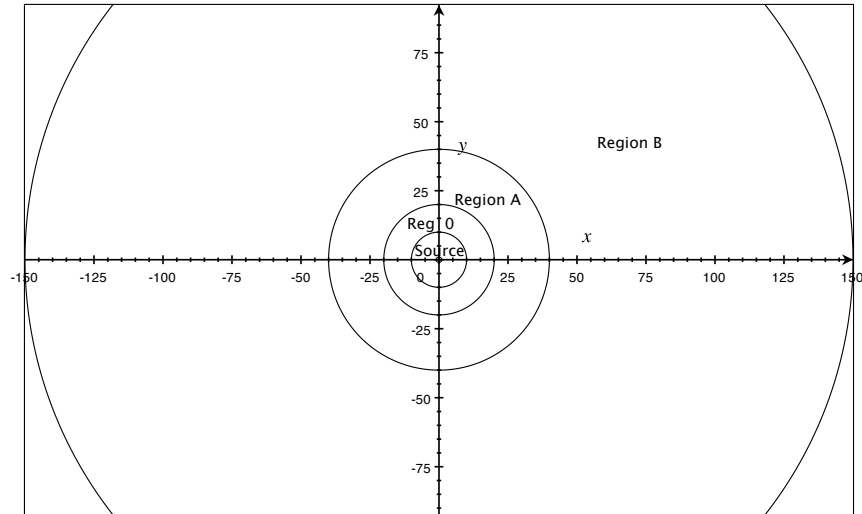


Figure 5.6: The regions defined by Olausen et al. (2011) for their analysis. Source I used is 0-1", source used by Olausen et al. is 0-10", region 0 is 10-20", region A is 20-40" and region B is 40-150".

5.4.2 Extended emission

I assume that the hydrogen column density is the same for the source as for the extended emission, $3.37 \times 10^{22} \text{ cm}^{-2}$. The extended emission is fitted with an absorption model with a power law. We see that the power law term Γ increases outwards. In the paper by Gaensler & Slane the best value for Γ for a pulsar wind nebula was around 2. This does not match the data here for these regions. Table 5.4.2 shows these values, fitted with XSpec model tbabs. The different regions were fitted simultaneously, since they all should have the same hydrogen column density. The data in the table gave a reduced χ^2 of 1.45.

	Γ	σ
Region 0	2.85	± 0.06
Region A	3.54	± 0.04
Region B	3.62	± 0.07

Table 5.4: Table of best fit parameters for the extended emission in different regions, all fitted with an absorption model and a power law.

I also made a spectrum from the extended emission from $1''$ to $200''$. This included the line in the image, running from upper left to lower right part of the image. In the background this line is also included, so this should not cause any problem. In this case we found $\Gamma = 3.23 \pm 0.03$ with a reduced χ^2 of 1.23.

This also does not agree with the factor 2 for Γ expected for a pulsar wind nebula.

5.5 Flux

From the best fit of the spectrum, XSpec can give an estimate of the flux. In plot 5.7 the flux of the source is plotted throughout time. In 2004 the flux was in a low state, in the next two years the flux went down a bit. Bernardini et al. (2011) made a distinction between different flux states of this magnetar. After this low state, the magnetar went into a medium flux state, where the flux increased by approximately a factor of 20 in 2007. Just after the burst of 2008, the flux increased even further into the high state. But the highest flux measured so far was in 2009, again just after the bursts. In the following year the flux decreased again. And also in 2011, the data inspected here, the flux decreased a bit. The different states were empirically selected by Bernardini et al. The flux was still very high during the observation of 2011. The decrease after the 2009 outburst ceased a bit. This was the reason I checked for outbursts prior to the observation, but no burst was detected by any telescope. This therefore will not be the reason for the higher flux.

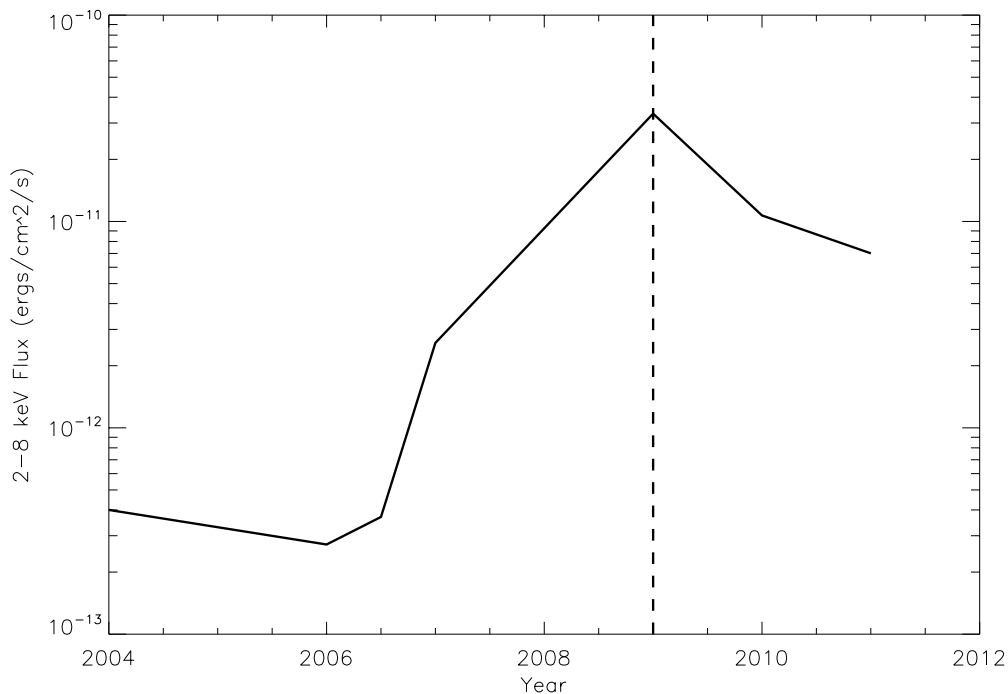


Figure 5.7: Flux of the source as a function of time, taken from different papers. Flux in 2-8 keV range increases towards the outbursts in 2008 and 2009.

But also for the full extended emission I can get the flux the same way we did for the source. The flux of the emission can also be compared to older measurements. Now we have a flux of 3.54×10^{-12} ergs s⁻¹ cm⁻². This is an increase compared to 2006 when Vink & Bamba 2009 found a flux of $1.0 \pm 0.3 \times 10^{-13}$ ergs s⁻¹ cm⁻² for the extended emission using Chandra and Olausen et al. 2011 found a flux of 4×10^{-14} ergs s⁻¹ cm⁻² for 2006 for XMM and 3.0×10^{-12} ergs s⁻¹ cm⁻² after the 2009 burst, all in 2-10 keV band.

And we see that the flux of the emission, between 1.5 and 7 keV, increases outwards.

Table 5.5 gives an overview of all fluxes at different energy bands for the source (of 1", not 10" as used by (Olausen et al., 2011)) and 3 regions as defined before.

Flux ($\times 10^{-13}$ ergs s ⁻¹ cm ⁻²)				
Energy	Source	Reg0	Reg A	Reg B
1 - 3	10.38	1.63	2.63	4.51
1.5 - 7	44.02	4.43	5.39	8.78
3 - 6	33.76	2.43	3.20	5.17
2 - 8	70.10	4.38		

Table 5.5: Table of the flux of the source and extended emission in 2011.

5.6 Hardness ratios

In the paper by Olausen et al. (2011) the pulsar wind nebula theory is dismissed. To compare the new data with their data and conclusions, we will also look at the hardness ratios calculated there. They looked at hardness ratios defined as $HR_{\text{ext}} \equiv I_{\text{ext}}(3-6 \text{ keV}) / I_{\text{ext}}(1-3 \text{ keV})$ and $HR_{\text{ps}} \equiv I_{\text{ps}}(3-6 \text{ keV}) / I_{\text{ps}}(1-3 \text{ keV})$, where ‘ext’ is for the extended source and ‘ps’ for the point source. Here I will repeat these calculations with energy bands of 1.5 - 3 keV and 3 - 7 keV and for the regions A and B and the source as defined in that paper.

Table 5.6 shows the hardness ratios as calculated by Olausen et al. for 2006 - 2010 and the calculation done for 2011. As in 2007 - 2010, the source emission was harder than that of the extended emission.

Observation	Hardness ratio		
	Point source	Region A	Region B
2006	0.306	0.21	0.46
2007	0.482	0.18	0.32
2009	1.014	0.55	0.45
2010	0.814	0.34	0.37
2011	1.63	0.64	0.61

Table 5.6: Hardness ratios for all regions from 2006 to 2011.

In 2006 the ratio was higher in region B than at the source. This is not the case in any other data set. In 2009 and 2011 $HR > 1$; meaning that the intensity of 3-7 keV was higher than for 1.5-3 keV. In 2011, for region 0, the hardnessratio is 0.81.

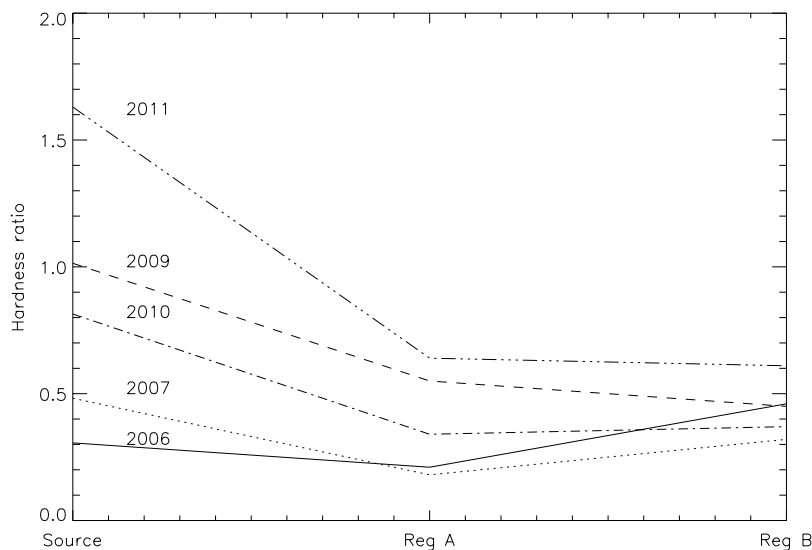


Figure 5.8: The hardness ratios according to Olausen et al., including the hardness ratio for 2011 data.

5.7 Fractional intensity

I also calculated the fractional intensity of the extended emission $I_{\text{frac}} = I_{\text{ext}} / I_{\text{ps}}$ for regions A and B. In figure 5.9 the fractional intensity from Olausen is plotted with the inclusion of the fractional intensity of the 2011 data. In region A we see the same behavior as in 2006, a higher intensity from the extended source, compared to the years after. But for region B we see the same behavior as 2007 to 2010, still a low intensity from the extended source in that region.

In the case of dust scattering, we would expect this to be constant. The amount of dust between us and the source does not change. If the star was brighter at some point, the dust scattering intensity would be higher, but also the point source intensity would be higher and this will cancel each other out. But there is a difference at the 2006 and 2011 observations. This can be explained by an extra component causing the extended emission to be lower and thus giving a higher fractional intensity. For 2011, in region 0, the fractional intensity is 0.05. Lower than in region A.

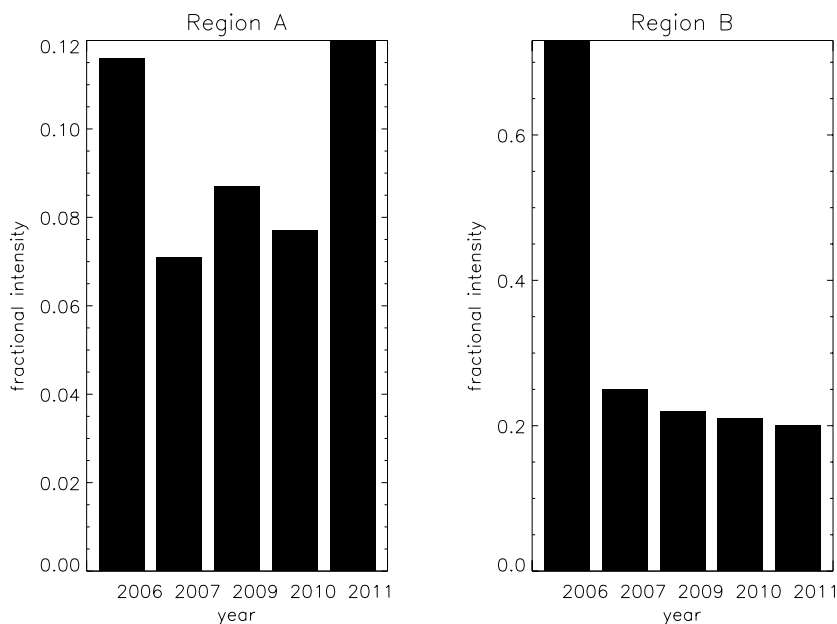


Figure 5.9: Fractional intensity over the years. Data for 2006-2010 from Olausen et al. 2011. And included the fractional intensity for 2011. In region A an extra component, on top of dust scattering, might explain I_{frac} , but this is not necessary for region B.

5.8 Radial profile

The main goal of this research is to find out if the extended emission is a pulsar wind nebula or if it is dust scattering. When having a look at the radial profile, which is a plot of the intensity as a function of radius, we can draw conclusions. There are some dust scattering models, of which one is used here. If the data and this model fit very well, we can assume the extended emission to be dust scattering. But if there is no good fit, we might conclude that there is something extra that is radiating. The radial profile will also give information about the distribution of the emission, to where it extends and if there is a peak at a certain radius.

First I created an exposure corrected image and a counts image which shows the number of counts in each pixel. For this I used different energy bands (table 5.7), to get a better insight on the energy dependence of the profile. Using CIAO I created a radial profile with these counts images. The source is the inner 1" (which was excluded for the radial profile because we are investigating the extended emission) and the extended emission is from 1" to 200", divided into annuli of 0.1". CIAO creates a radial profile by determining the net counts in all these concentric annuli and then dividing by the respective areas. This is the surface brightness and is a function of the radius.

number	Low	High	Weighted average
1	0.500	- 1.311 keV	0.91 keV
2	1.311	- 1.849 keV	1.63 keV
3	1.311	- 6.999 keV	3.10 keV
4	1.850	- 2.999 keV	2.37 keV
5	3.000	- 4.499 keV	3.63 keV
6	4.500	- 6.999 keV	5.62 keV
7	6.000	- 6.999 keV	6.52 keV
8	6.000	- 10.00 keV	8.66 keV
9	7.000	- 10.00 keV	8.89 keV

Table 5.7: All different energy bands defined at the beginning, from which only numbers 2-5 were used. There were not much photons in the lower and higher energy bands. But this had to be checked.

From all these radial profiles it was clear that there were not much counts at energies high than 7.0 keV or below 1.311 keV. Therefore I continued with the radial profiles with number 3,4,5,6 for further investigation. There was much data, 1990 annuli and thus 1990 data points, so I did some rebinning at higher radii by taking 2 points and taking their average in radius and intensity and recalculating the error. The amount of rebinning was done by eye, for a clearer image.

5.8.1 Draine model

The dust scattering model I used for the radial profile is the dust scattering model from Draine (2003). This model is based on interstellar dust grains, despite their uncertain nature (see section 4.2.2). The dust grains can absorb and scatter X-rays and result in a halo of scattering around the source. Here is assumed that the grains can be approximated as homogeneous spheres. The scattering is dominated by dust grains containing $> 10^6$ atoms and with radii > 100 Å.

The model uses the median scattering angle for photons with energy E where for $E > 0.5$ keV:

$$\theta_{s,50} \approx 360'' \left(\frac{\text{keV}}{E} \right). \quad (5.1)$$

Here we make a simple approximation for the differential scattering cross section:

$$\frac{d\sigma}{d\Omega} \approx \frac{\sigma_{\text{sca}}}{\pi\theta_{s,50}^2} \frac{1}{[1 + (\theta/\theta_{s,50})^2]^2}. \quad (5.2)$$

If we assume the halo angle to be approximately

$$\theta_h \approx (1 - x)\theta_s \quad (5.3)$$

for small angles, which we assume since the halo of scattered X-rays is within 1° of the X-ray source. Here $0 \leq x \leq 1$ and $r = xD$ with D the distance to the source.

The fraction of halo photons within θ_h is defined as

$$g(\theta_h) \equiv \frac{N_{\text{halo}}(< \theta_h)}{N_{\text{halo}}}. \quad (5.4)$$

If a plane-parallel perpendicular dust density is assumed,

$$g(\theta_h) \equiv \int_0^1 dx \tilde{\rho}(x) \frac{\sigma_{\text{sca}}[< \theta_h/(1-x)]}{\sigma_{\text{sca}}}, \quad (5.5)$$

where $\tilde{\rho}$ is the dimensionless normalized dust density along the line of sight.

If we assume a uniform dust scattering gradient ($\tilde{\rho}(x) = (1 - \beta) + 2\beta x$) we get

$$g(\theta_h) = (1 + \beta) \frac{\theta_h}{\theta_{s,50}} \arctan \left(\frac{\theta_{s,50}}{\theta_h} \right) - \beta \left(\frac{\theta_h}{\theta_{s,50}} \right)^2 \ln \left[1 + \left(\frac{\theta_{s,50}}{\theta_h} \right)^2 \right], \quad (5.6)$$

where we assume $\beta = 1$ (3/4 of the dust near the source) since the source is in the galactic plane, towards the galactic center.

We also know that

$$g(\theta_h) = \int \Sigma(\theta_h) 2\pi\theta_h d\theta_h, \quad (5.7)$$

where Σ the radial profile is, so

$$\Sigma(\theta_h) = \frac{1}{2\pi\theta_h} \frac{dg(\theta_h)}{d\theta_h}. \quad (5.8)$$

$$\Sigma(r) = \frac{1}{2\pi r} \left(\frac{1 + \beta}{\theta_{s,50}} \arctan \left(\frac{\theta_{s,50}}{r} \right) + \frac{\beta}{r} \frac{1}{1 + \left(\frac{\theta_{s,50}}{r} \right)^2} - \frac{2\beta r}{\theta_{s,50}^2} \ln \left[1 + \left(\frac{\theta_{s,50}}{r} \right)^2 \right] \right) \quad (5.9)$$

In this last equation I replaced θ_h with r (for radius) because this is the profile I will fit to the data as a function of angular radius.

5.9 Radial profile

5.9.1 2011 data

In figures 5.10 and 5.11 we see the radial profiles of energy bands 1.85 - 3.0 keV, 1.3 - 7.0 keV, 3.0 - 4.5 keV and 4.5 - 7.0 keV. The errors on the data are much smaller than the characters (X) used to show the data points. They are too small to show up in the figures. The dust scattering model of Draine is correct except for a normalization factor. This factor is found by minimizing $\frac{\text{data} - \text{norm} \times \text{model}}{\text{error}}$ for all 4 energy ranges:

energy (keV)	norm
1.85 - 3.0	8846.9
1.3 - 7.0	15896.5
3.0 - 4.5	4233.0
4.5 - 7.0	909.97

Table 5.8: The energy bands used and the normalization factor for the dust scattering model from Draine (2003).

(where ‘norm’ is the normalization factor.)

Figure 5.10 shows the data for the different energy bands and the best fit of the model. In general the shape of the data is comparable to the model. The first part is still from the PSF of Chandra and after that the model is a reasonable fit. As we look at the data for the 4.5 - 7.0 keV band, we see some features that do not fit the line of the model.

We can also make one fit for all energy bands with the same normalization factor. Then the best fit is for the model with a factor of 5700.0, see figure 5.11. At full energy band from 1.5 - 7.0 keV the model falls below the observations, for 3.0 - 4.5 keV it gives the best fit and at higher energies the model overestimates the amount of dust scattering.

With the equations, tables and figures from the paper of Draine I was able to examine some properties of the dust with the help of the dust scattering model.

	2006	2011
Source (1") flux	2.7×10^{-13}	7.01^{-13}
Extended flux	1.0×10^{-13}	1.75^{-13}
f_{halo}	0.27	0.20
τ_{sca}	0.31508	0.22
n_{H}	3.25×10^{22}	3.58×10^{22}
σ_{sca}	9.70×10^{-24}	6.23×10^{-24}

Table 5.9: Some properties for 2006 and 2011 with the use of the radial profile and equations, tables and figures in Draine (2003).

5.10 Rings

In 2009 dust rings were visible in the observations after the burst. They showed up in the radial profile as clear peaks. One of the possibilities of an excess of scattering in the 2006 data was that there were rings in the field (see section 4.4).

In the 2011 data there were no rings visible. Not in the observation, but also not in the radial profile. Therefore we conclude that there were no rings of dust at that time that could explain the abnormalities.

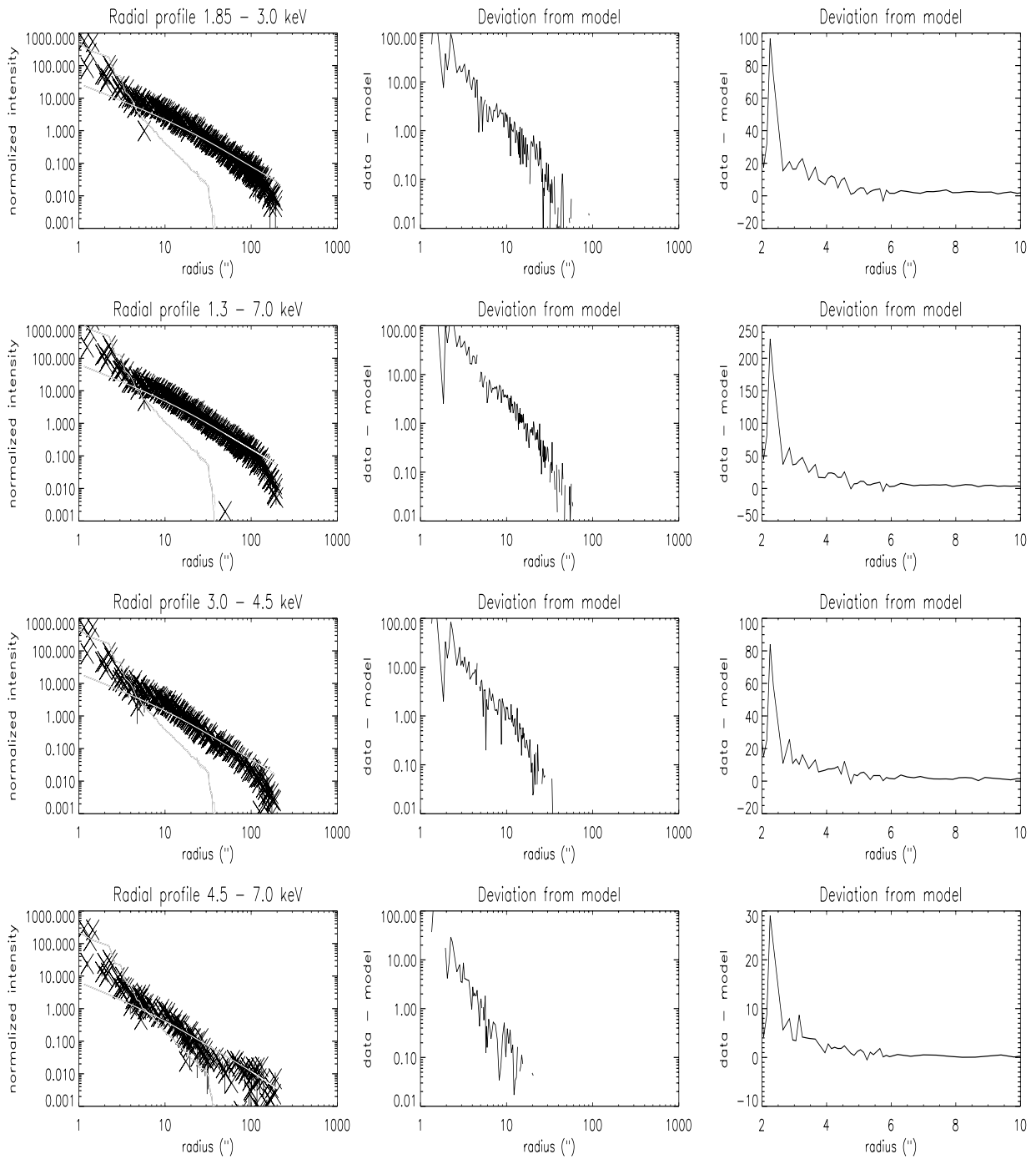


Figure 5.10: Radial profiles with the best fit of the Draine dust scattering model for **different** normalization factors for energy bands 1.85 - 3.0 keV, 3.0 - 4.5 keV, 4.5 - 7.0 keV and 1.3 - 7.0 keV. First: the data points at different energies shown in X, the psf and model are the lines in grey. Middle: difference between model and data in logarithmic plot. Right: difference between model and data.

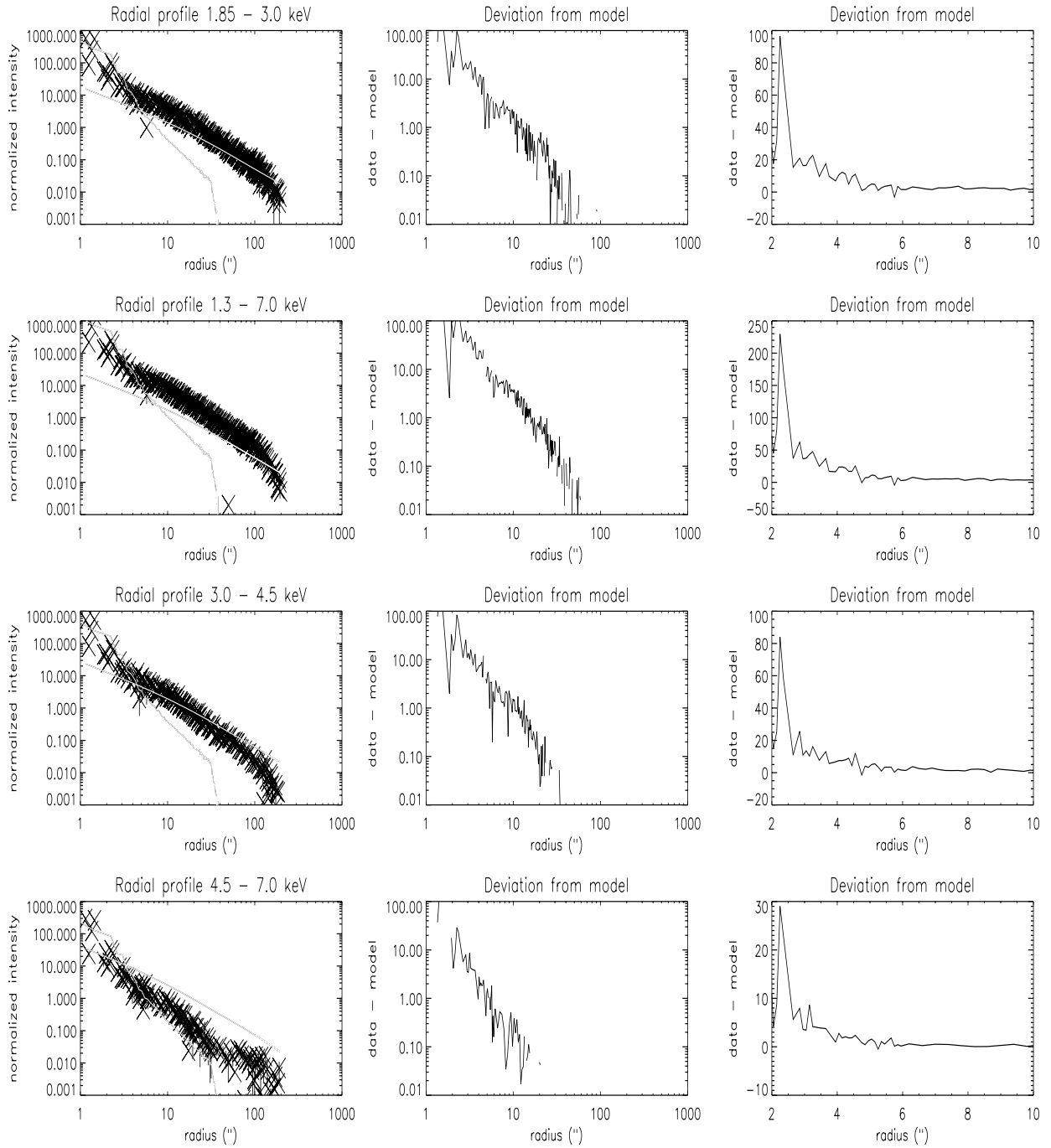


Figure 5.11: Radial profiles with the best fit of the Draine dust scattering model for the **same** normalization factor for energy bands 1.85 - 3.0 keV, 3.0 - 4.5 keV, 4.5 - 7.0 keV and 1.3 - 7.0 keV. First: the data points at different energies shown in X, the psf and model are the lines in grey. Middle: difference between model and data in logarithmic plot. Right: difference between model and data.

Chapter 6

Discussion

The main problem with this observation was that the source was very bright. For a short and less detailed observation this would not give any problems, but this is a longer observation to get a good look at the source.

Due to the brightness of the source, the detector was saturated, so we also had to take pile-up into account during the analysis. XSpec can take the pile-up into account through a model, but this is also not perfect. This will give uncertainties in the best fit of the spectrum and thus in the flux, hardness ratio and fractional intensity.

The dust scattering model from Draine (2003) overestimates the amount of dust scattering. It is not perfect. Observations by Smith (2008) showed the poor fit of the model. A better dust scattering model should be able to give a more conclusive answer.

To help understand the pulsar wind nebula, Vink, Haverkorn & Bamba proposed to observe the magnetar in radio. With this they want to confirm the existence of the nebula, discovered in X-rays, and create a detailed spectral index map of the nebula. The data should tell something about the formation of the PWN, was it formed like other PWNe powered by the spin down or was it due to bursts? These data are not yet available, but this is a good future research project.

Also new X-ray data from when the source is in a quiescent state again would give more information. Now the source is bright, but also the dust surrounding the source is lit up. This makes it more difficult to observe a possible pulsar wind nebula.

And a better understanding of magnetars in general would give answers to many unknown characteristics of the source. What is normal and what is abnormal for magnetars and how are they different from normal pulsars. These are some unanswered questions that might help in further investigations.

Chapter 7

Conclusions

The main goal of this project was to figure out if the extended emission around magnetar 1E1547.0-5408 is dust scattering of a pulsar wind nebula. We did this by comparing the 2011 X-ray data with a dust scattering model and by looking at the spectrum, hardness ratio and fractional intensity.

The dust scattering model by Draine showed that the overall shape of the radial profile in 2011 is the same as for dust scattering. From 2" - 5" there is an excess of photons, but beyond this point the model fits very well. From this we can conclude that there might be an extra component near the source, but not for the rest of the emission.

From the fractional intensity ($\frac{I_{\text{ext}}}{I_{\text{ps}}}$) we see some peculiarities. The original paper this research was based on, used data from 2006. At that time the fractional intensity was high in both regions A and B and one could conclude there is more than dust scattering. But in the following years, until 2010, this fraction was low again and no extra component, beside dust scattering, is needed to explain the observations. In 2011 the fractional intensity in region A was high again, but not in region B. From this we could conclude there is something more than just dust scattering for the inner part of the extended emission, but not beyond 40".

The hardness ratio is also very interesting. In 2009 the HR was different from other observations, most likely due to the outburst. But in 2011 the HR for the source was larger than 1, meaning that the intensity at 3-7 keV is larger than at 1.5-3 keV. For regions A and B the HR was higher than ever measured before. But it is hard to get conclusions since the source was very bright during the observation.

I would say there is something going on with this source, whether there is a pulsar wind nebula or dust scattering. But from this research project I cannot give a conclusive answer.

We can conclude that magnetar 1E1547.0-5408 is a very interesting magnetar to study. It is the one with the fastest rotation, the highest magnetic field, one of only two known radio magnetars and there are hints for a PWN.

Bibliography

- Bernardini, F., Israel, G. L., Stella, L., Turolla, R., Esposito, P., Rea, N., Zane, S., Tiengo, A., Campana, S., Gtz, D., Mereghetti, S., Romano, P., 2011, *A&A*,529A,19B
- Camilo, F., Ransom, S. M., Halpern, J. P., Reynolds, J., 2007, *ApJ*, 666, L93
- Cordes, J.M. & Lazio, T.J.W., 2002, *astro-ph*,7156
- Cordon & Ransom on www.cv.nrao.edu/course/astr534/Pulsars.html
- Davis, J.E., 2001, *ApJ*, 562,575-582
- Dib, Rim, Kaspi, Victoria M., Scholz, Paul, Gavriil, Fotis P., 2012, *ApJ*, 748,3
- Draine, B.T., 2003, *ApJ* 598:1026-1037
- Draine, B.T., 2003, *ARAA*,41,241
- Fruscione et al. 2006, *SPIE*, 6270, 60
- Gaensler, B.M. & Slane, P.O., 2006, *ARA&a*, 44, 17G
- Gelfand, J.D. & Gaensler, B.M.,2007,*ApJ*,667:1111-1118
- Gordon, K.D.,2004,*ASPC*,309,77G
- Gotthelf, E.V.,2004,*IAUS*,218,225
- Kargaltsev,O. & Pavlov, G.G.,2008,*AIPC*,983,171
- Kaspi, V.M.2007,*Ap&SS*,308,1
- Kouveliotou, C., Duncan, R.C. and Thompson, C,2003, *Scientific American* Feb 2003
- Kuiper, L., Hermsen, W., den Hartog, P. R., Urama, J. O.,2012, *ApJ*,748,133K
- Lamb, R.C. & Markert, T.H.,1981, *ApJ*, 244, 94
- Lorimer, D. & Kramer, M.,2005, *Handbook of Pulsar Astronomy*, Cambridge University Press
- Mereghetti, S.,2008, *A&ARv*,15,225M
- Nobili, L., Turolla, R., Zane,S.,2008, *MNRAS*, 389, 989

Olausen, S. A., Kaspi, V. M., Ng, C.-Y., Zhu, W. W., Dib, R., Gavriil, F. P., Woods, P. M.,2011, ApJ, 742, 40

Predehl, P. & Schmitt, J.H.M.M.,1995, A&A, 293, 889-905

Ruderman, M., 1969, Nature, 223,597-598

Slane, P.O.,2008, AIPConf.Proc.968:143-150

Smith, R.K.,2008, ApJ, 681:343-349

Smith, R.K. & Dwek, E.,1998, ApJ, 503, 831:842

Thompson, C. & Duncan, R.C.,1993, ApJ, 408, 194

Tiengo, A., Vianello, G., Esposito, P., Mereghetti, S., Giuliani, A., Costantini, E., Israel, G. L., Stella, L., Turolla, R., Zane, S., Rea, N., Gtz, D., Bernardini, F., Moretti, A., Romano, P., Ehle, M., Gehrels, N.,2010, ApJ, 710, 227T

Vink, J. & Kuiper, L.,2006, MNRAS, 370, L14

Vink, J. & Bamba, A.,2009, ApJ, 707:L148-L152

Vink, J., Haverkorn, M., Bamba, A.,2010, Proposal ATCA

Vink, J., Bamba, A., Yamazaki, R.,2011, ApJ, 727,131